Edge of Chaos Induces a Hopf Bifurcation in a Bio-Inspired Thermally-Activated Memristor Oscillator

Edge of Chaos Induces a Hopf Bifurcation in a Bio-Inspired Thermally-Activated Memristor Oscillator

A. Ascoli, E. Gemo, D. Rossetti, F. Corinto, M. Bonnin, M. Gilli, P.P. Civalleri
Department of Electronics and Telecommunications, *Politecnico di Torino*, Torino, Italia
alon.ascoli@polito.it

A.S. Demirkol, N. Schmitt, I. Messaris, V. Ntinas, D. Prousalis, R. Schroedter, R. Tetzlaff
Institut für Grundlagen der Elektrotechnik und Elektronik, *TU Dresden*, Dresden, Germany

S. Slesazeck[a], T. Mikolajick[a,b]
[a] NaMLab gGmbH, [b] *Institut für Halbleiter- und Mikrosystemtechnik*, *TU Dresden*, Dresden, Germany

L. Chua
Department of Electrical Engineering and Computer Sciences, *University of California, Berkeley*, Berkeley, California, USA

***Abstract*— This manuscript sheds light into the fundamental importance of the Principles of Local Activity and Edge of Chaos for the future design of innovative circuits, which, employing biomimetic memristive devices, are ideally suited for the development of energy-efficient artificially-intelligent technical systems. The focus of the work is the design of a Second-Order Reactance-Less Oscillator, across which oscillations may develop if and only if at least one of its two different volatile thermally-activated memristor physical realizations is biased along a negative differential resistance branch of the respective DC locus, which turns it into a source of local energy. Very importantly, the proposed cell is first found to lock in the oscillatory mode out of a local Hopf Supercritical Bifurcation when its design parameters are chosen from the Edge of Chaos region, providing clear evidence for the high degree of excitability it acquires as a result.**

Keywords—Edge of Chaos, Local Activity, Negative Differential Resistance, Memristors, Reactance-Less Thermally-Activated Memristor Oscillators, Energy-Efficient Bio-Inspired Electronics, Artificial Intelligence Edge Computing Applications

I. INTRODUCTION

The focus of the scientific community is currently directed intensively and extensively on disruptive nanoscale memristive devices, which, featuring rather unique properties, promise to boost the performance of technical systems for *Artificial Intelligence* applications, allowing especially the implementation of energy-efficient *Edge Computing* paradigms. While nonvolatile memristors are typically employed as programmable resistors arranged in dense crossbar arrays to accelerate matrix-vector multiplications, i.e. the basic operations in machine learning algorithms, or, alternatively, to store data in resistance form, allowing the physical realization of in-memory computing paradigms, the potential of biomimetic volatile memristors [1]-[3] endowed with *Local Activity* [4], i.e. the capability to act as sources of small-signal or infinitesimal or local energy under suitable polarization, similarly as the ion channels in neuronal membranes, to boost the energy efficiency and data-processing functionalities of electronic circuits so to address the *Industry 4.0* demanding needs, is yet to be fully uncovered.

Recently, the extremely-rich nonlinear dynamics of memristive nanodevices of this kind [5], especially as they operate on the stable part of their local activity domain, referred to as *Edge of Chaos* [6], has been leveraged in various works to reproduce complex phenomena, including symmetry-breaking effects [7] and vital neuronal bifurcations [8], emerging across high-order biological systems through lower-order electrical circuits, which clearly shed light into the captivating opportunities they open up in the field of energy-efficient bio-inspired electronics [9].

Recently, we showed how a simple second-order electrical network, composed of two identical and diffusively-coupled reaction cells, each of which including one niobium oxide (NbOx) memristor [5] from NaMLab [10] and one DC current source only, is capable to support static pattern formation via Turing instability as the passive and linear coupling resistance is decreased below a critical local bifurcation threshold, provided the single cell is poised on the Edge of Chaos on its own [11]. The reactance-less reaction-diffusion network was however unable to lock in some oscillatory operating mode. This paper presents an even simpler second-order analogue electronic cell, which requires just two distinct thermally-activated locally-active memristors, namely a current-controlled NbOx threshold nano-switch [5] from NaMLab and a voltage-contolled positive temperature coefficient (PTC) thermistor [12], and a couple of independent sources, generating a DC current and a DC voltage, respectively, to sustain steady-state limit-cycle oscillations. Critical to the oscillator design and at the origin for the use of two DC sources in its circuit is ensuring that the S-shaped DC locus of the current-controlled threshold switch may cross the N-shaped DC load line extracted from the DC locus of the voltage-controlled thermistor in such a way that at least one of the two memristors is poised at some Negative Differential Resistance operating point. Most importantly, an in-depth nonlinear circuit-theoretic analysis allows to demonstrate how fundamental is for the proposed cell to enter the excitability regime of the Edge of Chaos for the emergence of infinitesimally-small almost-sinusoidal oscillations across its circuit out of a local Hopf supercritical bifurcation [13]. A rigorous analysis of the local and global dynamics of the thermally-activated cell under sweep in either of the two bias sources allows to identify regions of the plane, spanned by these two parameters, endowing it with an oscillatory *modus operandi*, which correspondingly allows to optimize the design so as to prevent nonidealities to ever quench the oscillations. Before devoting efforts to realize the oscillator in hardware, we shall next investigate whether the use of other locally-active memristor physical realizations may allow to simplify the bias circuitry of the proposed cell, while concurrently enlarging the region of the design parameter space where it operates as desired. The ultimate goal of this research is to identify bio-inspired circuit topologies which may be integrated densely across artificial neural networks and solve challenging problems through

some intelligent and energy-efficient form while operating on the Edge of Chaos, which could be triggered by opportune stimuli at regular time intervals or on demand.

II. MODELS OF MEMRISTORS ON EDGE OF CHAOS

The next two sections present the two memristors on Edge of Chaos [14] to be employed later on for the design of a second-order reactance-less thermally-activated oscillator.

A. THE PTC THERMISTOR

The nonlinear dynamics of a voltage-controlled PTC thermistor $\mathcal{M}_T$ may be described by the combination between an ordinary differential equation (ODE) of the form [12]

$$\dot{T} = \dot{T}(T, v_{\mathcal{M}_T}) = \delta \cdot H_C^{-1} \cdot (T_0 - T) + G_{\mathcal{M}_T}(T) \cdot H_C^{-1} \cdot v_{\mathcal{M}_T}^2, \quad (1)$$

and an algebraic constraint reading as

$$i_{\mathcal{M}_T}(T, v_{\mathcal{M}_T}) = G_{\mathcal{M}_T}(T) \cdot v_{\mathcal{M}_T}, \quad (2)$$

where the device temperature T encodes its volatile state, $v_{\mathcal{M}_T}$ and $i_{\mathcal{M}_T}$ stand for its voltage and current respectively, whereas $G_{\mathcal{M}_T}(T)$, denoting its memductance function, is given by

$$G_{\mathcal{M}_T}(T) = G_O \cdot \exp(-\beta \cdot (T - T_0)). \quad (3)$$

The values for the model parameters δ, H_C, T_0, G_0 and β are reported in Table I.

Table I. PTC thermistor model parameter setting. Physical units are omitted.

δ	H_C	T_0	G_O	β
48	$4.8 \cdot 10^{-7}$	300	1.5	$10 \cdot 10^3$

The DC current $I_{\mathcal{M}_T,eq}$ versus voltage $V_{\mathcal{M}_T,eq}$ characteristic of the PTC thermistor is shown in Fig. 1, where a magenta (blue) branch includes DC bias points, where the device admits a positive (negative) differential resistance, referred to via the acronym PDR (NDR) in the remainder of this manuscript.

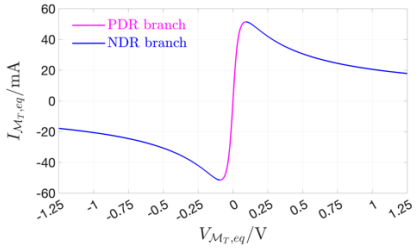

Fig. 1 DC $I_{\mathcal{M}_T,eq}$ versus $V_{\mathcal{M}_T,eq}$ characteristic of the voltage-controlled PTC thermistor. Each bias point $\boldsymbol{P}_{\mathcal{M}_T} = (V_{\mathcal{M}_T,eq}, I_{\mathcal{M}_T,eq})$ is unequivocally associated to a device operating point $Q_{\mathcal{M}_T} \triangleq T_{eq}$. The locus of the voltage-controlled device has a N shape on the first quadrant of the $I_{\mathcal{M}_T,eq}$ versus $V_{\mathcal{M}_T,eq}$ plane.

Table II reports the expressions for the PTC thermistor local model parameters as a function of the respective operating point $Q_{\mathcal{M}_T}$.

Table II. PTC thermistor local model coefficients about $Q_{\mathcal{M}_M}$.

$a_{\mathcal{M}_T,Q_{\mathcal{M}_T}} \triangleq (\partial \dot{T}/\partial T)\big\vert_{Q_{\mathcal{M}_T}}$	$b_{\mathcal{M}_T,Q_{\mathcal{M}_T}} \triangleq (\partial \dot{T}/\partial v_{\mathcal{M}_T})\big\vert_{Q_{\mathcal{M}_T}}$
$-(\beta \cdot G_{\mathcal{M}_T}(T_{eq}) \cdot V_{\mathcal{M}_T,eq}^2 + \delta) \cdot H_C^{-1}$	$2 \cdot V_{\mathcal{M}_T,eq} \cdot G_{\mathcal{M}_T}(T_{eq}) \cdot H_C^{-1}$
$c_{\mathcal{M}_T,Q_{\mathcal{M}_T}} \triangleq (\partial i_{\mathcal{M}_T}/\partial T)\big\vert_{Q_{\mathcal{M}_T}}$	$d_{\mathcal{M}_T,Q_{\mathcal{M}_T}} \triangleq (\partial i_{\mathcal{M}_T}/\partial v_{\mathcal{M}_T})\big\vert_{Q_{\mathcal{M}_T}}$
$-\beta \cdot G_{\mathcal{M}_T}(T_{eq}) \cdot V_{\mathcal{M}_T,eq}$	$G_{\mathcal{M}_T}(T_{eq})$

One of the possible circuit representations of the device small-signal model about $Q_{\mathcal{M}_T}$ is shown in Fig. 2(a).

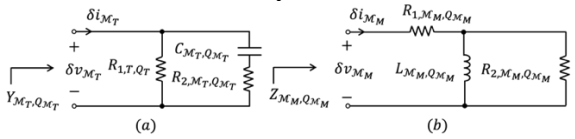

Fig. 2 A possible circuit-theoretic representation of the local model of the voltage-controlled PTC thermistor about $Q_{\mathcal{M}_T}$ (a), and of the current-controlled NaMLab NbOx memristor about $Q_{\mathcal{M}_M}$ (b) [15].

The local admittance $Y_{Q_{\mathcal{M}_T}}$ of $\mathcal{M}_T$ about $Q_{\mathcal{M}_M}$ may be expressed as

$$Y_{Q_{\mathcal{M}_T}}(s) = K_{Y_{Q_{\mathcal{M}_T}}} \cdot \frac{s - z_{Y_{Q_{\mathcal{M}_T}}}}{s - p_{Y_{Q_{\mathcal{M}_T}}}}, \quad (4)$$

where the formulas for the scaling factor, the zero and the pole are given in Table II.

Table II. Formulas for scaling factor, zero and pole of the admittance of the cell in (a) at the respective input port about $Q_{\mathcal{M}_T}$.

$K_{Y_{Q_{\mathcal{M}_T}}} = 1/(R_{1,\mathcal{M}_T,Q_{\mathcal{M}_T}} \parallel R_{2,\mathcal{M}_T,Q_{\mathcal{M}_T}})$
$z_{Y_{Q_{\mathcal{M}_T}}} = -1/(C_{\mathcal{M}_T,Q_{\mathcal{M}_T}} \cdot (R_{1,\mathcal{M}_T,Q_{\mathcal{M}_T}} + R_{2,\mathcal{M}_T,Q_{\mathcal{M}_T}}))$
$p_{Y_{Q_{\mathcal{M}_T}}} = -1/(C_{\mathcal{M}_T,Q_{\mathcal{M}_T}} \cdot R_{2,\mathcal{M}_T,Q_{\mathcal{M}_T}})$
$R_{1,\mathcal{M}_T,Q_{\mathcal{M}_T}} = a_{\mathcal{M}_T,Q_{\mathcal{M}_T}}/(a_{\mathcal{M}_T,Q_{\mathcal{M}_T}} \cdot d_{\mathcal{M}_T,Q_{\mathcal{M}_T}} - b_{\mathcal{M}_T,Q_{\mathcal{M}_T}} \cdot c_{\mathcal{M}_T,Q_{\mathcal{M}_T}})$
$R_{2,\mathcal{M}_T,Q_{\mathcal{M}_T}} = a_{\mathcal{M}_T,Q_{\mathcal{M}_T}}/(b_{\mathcal{M}_T,Q_{\mathcal{M}_T}} \cdot c_{\mathcal{M}_T,Q_{\mathcal{M}_T}})$
$C_{\mathcal{M}_T,Q_{\mathcal{M}_T}} = -b_{\mathcal{M}_T,Q_{\mathcal{M}_T}} \cdot c_{\mathcal{M}_T,Q_{\mathcal{M}_T}}/a_{\mathcal{M}_T,Q_{\mathcal{M}_T}}^2$

It may be demonstrated that $R_{2,\mathcal{M}_T,Q_{\mathcal{M}_T}}$ and $C_{\mathcal{M}_T,Q_{\mathcal{M}_T}}$ are always positive irrespective of $Q_{\mathcal{M}_T}$. On the other hand, $R_{1,\mathcal{M}_T,Q_{\mathcal{M}_T}}$ is negative at any operating point $Q_{\mathcal{M}_T}$ corresponding to a NDR bias point $\boldsymbol{P}_{\mathcal{M}_T}$, whereas it is positive elsewhere. Observing also that $R_{1,\mathcal{M}_T,Q_{\mathcal{M}_T}} + R_{2,\mathcal{M}_T,Q_{\mathcal{M}_T}}$ features the same polarity as $R_{1,\mathcal{M}_T,Q_{\mathcal{M}_T}}$ for any $Q_{\mathcal{M}_T}$, the application of the Local Activity Theorem and of the Edge of Chaos Corollary [6] allows to conclude that the voltage-controlled PTC thermistor may only operate on the Edge of Chaos at some operating point $Q_{\mathcal{M}_T}$ where concurrently the two inequalities $p_{Y_{Q_{\mathcal{M}_T}}} < 0$ and $z_{Y_{Q_{\mathcal{M}_T}}} > 0$ apply, which is the case if and only if $\boldsymbol{P}_{\mathcal{M}_T}$ lies on the NDR branch of the $I_{\mathcal{M}_T,eq}$ versus $V_{\mathcal{M}_T,eq}$ locus.

B. THE NIOBIUM OXIDE THRESHOLD NANO-SWITCH

The model [5] of a NbOx threshold nano-switch $\mathcal{M}_M$, manufactured at NaMLab [10], combines a state equation of the form

$$\dot{x} = \dot{x}(x, v_{\mathcal{M}_M}) = a_0 + a_1 \cdot x + (b_2 + c_{21} \cdot x + c_{22} \cdot x^2 + c_{23} \cdot x^3 + c_{24} \cdot x^4 + c_{25} \cdot x^5) \cdot v_{\mathcal{M}_M}^2, \quad (5)$$

and an Ohm-based law reading as

$$i_{\mathcal{M}_M} = i_{\mathcal{M}_M}(x, v_{\mathcal{M}_M}) = G_{\mathcal{M}_M}(x) \cdot v_{\mathcal{M}_M}, \quad (6)$$

where x encodes the volatile state of the device, $i_{\mathcal{M}_M}$ ($v_{\mathcal{M}_M}$) denotes the current (voltage) flowing (falling) through (across) its physical stack, while $G_{\mathcal{M}_M}(x)$, standing for its memductance function, admits the formula

$$G_{\mathcal{M}_M}(x) = d_0 + d_1 \cdot x + d_2 \cdot x^2 + d_3 \cdot x^3 + d_4 \cdot x^4. \quad (7)$$

Despite the voltage variable v_M appears on the right-hand sides of equations (5) and (7), the NaMLab memristor is a current-controlled device from a circuit-theoretic perspective. Table III reports the values of the model parameters a_0, a_1, b_2, c_{21}, c_{22}, c_{23}, c_{24}, c_{25}, d_0, d_1, d_2, d_3, and d_4.

Table III. NbOx switch model parameter setting. Physical units are omitted.

a_0	a_1	b_2	c_{21}	c_{22}	c_{23}	c_{24}
$5.19 \cdot 10^9$	$-2.05 \cdot 10^7$	$7.21 \cdot 10^9$	$-7 \cdot 10^7$	$2.27 \cdot 10^5$	-240	0.125

c_{25}	d_0	d_1	d_2	d_3	d_4
$-2.69 \cdot 10^{-5}$	$6.5 \cdot 10^{-3}$	$-6.66 \cdot 10^{-5}$	$2.14 \cdot 10^{-7}$	$-2.14 \cdot 10^{-10}$	$1.19 \cdot 10^{-13}$

The DC current $I_{\mathcal{M}_M,eq}$ versus voltage $V_{\mathcal{M}_M,eq}$ locus of the NaMLab memristor is illustrated in Fig. 2, where a black (red) branch includes DC bias points, where the device admits a PDR (NDR).

The formulas for the NaMLab memristor local model parameters as a function of the respective operating point $Q_{\mathcal{M}_M}$ are reported in Table IV. A possible circuit-theoretic representation of the NaMLab memristor local model about

$Q_{\mathcal{M}_M}$ is depicted in plot (b) of Fig. 2. The local impedance $Z_{Q_{\mathcal{M}_M}}$ of $\mathcal{M}_M$ about $Q_{\mathcal{M}_M}$ may be expressed as

$$Z_{Q_{\mathcal{M}_M}}(s) = K_{Z_{Q_{\mathcal{M}_M}}} \cdot \frac{s - z_{Z_{Q_{\mathcal{M}_M}}}}{s - p_{Z_{Q_{\mathcal{M}_M}}}}, \quad (8)$$

where the formulas for the scaling factor, the zero and the pole are given in Table V.

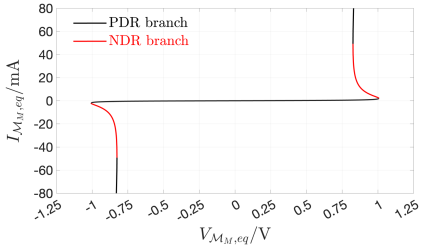

Fig. 2 DC $I_{\mathcal{M}_M,eq}$ versus $V_{\mathcal{M}_M,eq}$ characteristic of the NaMLab memristor. Each bias point $\boldsymbol{P}_{\boldsymbol{\mathcal{M}_M}} = (V_{\mathcal{M}_M,eq}, I_{\mathcal{M}_M,eq})$ is unequivocally associated to a device operating point $Q_{\mathcal{M}_M} \triangleq X_{eq}$. The locus of the current-controlled device has a S shape on the first quadrant of the $I_{\mathcal{M}_M,eq}$ versus $V_{\mathcal{M}_M,eq}$ plane.

Table IV. NaMLab memristor local model coefficients about $Q_{\mathcal{M}_M}$.

$a_{\mathcal{M}_M,Q_{\mathcal{M}_M}} \triangleq (\partial\dot{x}/\partial x)\vert_{Q_{\mathcal{M}_M}}$
$a_1 + V_{\mathcal{M}_M,eq}^2 \cdot (c_{21} + 2 \cdot c_{22} \cdot X_{eq} + 3 \cdot c_{23} \cdot X_{eq}^2 + 4 \cdot c_{24} \cdot X_{eq}^3 + 5 \cdot c_{25} \cdot X_{eq}^4)$
$b_{\mathcal{M}_M,Q_{\mathcal{M}_M}} \triangleq (\partial\dot{x}/\partial v_{\mathcal{M}_M})\vert_{Q_{\mathcal{M}_M}}$
$2 \cdot (b_2 + c_{21} \cdot X_{eq} + c_{22} \cdot X_{eq}^2 + c_{23} \cdot X_{eq}^3 + c_{24} \cdot X_{eq}^4 + c_{25} \cdot X_{eq}^5) \cdot V_{\mathcal{M}_M,eq}$
$c_{\mathcal{M}_M,Q_{\mathcal{M}_M}} \triangleq (\partial i_{\mathcal{M}_M}/\partial x)\vert_{Q_{\mathcal{M}_M}}$
$(d_1 + 2 \cdot d_2 \cdot X_{eq} + 3 \cdot d_3 \cdot X_{eq}^2 + 4 \cdot d_4 \cdot X_{eq}^3) \cdot V_{\mathcal{M}_M,eq}$
$d_{\mathcal{M}_M,Q_{\mathcal{M}_M}} \triangleq (\partial i_{\mathcal{M}_M}/\partial v_{\mathcal{M}_M})\vert_{Q_{\mathcal{M}_M}}$
$G_{\mathcal{M}_M}(X_{eq})$

Table V. Formulas for scaling factor, zero and pole of the impedance of the linear circuit in (b) at the respective input port about $Q_{\mathcal{M}_M}$.

$K_{Z_{Q_{\mathcal{M}_M}}} = R_{1,\mathcal{M}_M,Q_{\mathcal{M}_M}} + R_{2,\mathcal{M}_M,Q_{\mathcal{M}_M}}$
$z_{Z_{Q_{\mathcal{M}_M}}} = -(R_{1,\mathcal{M}_M,Q_{\mathcal{M}_M}} \parallel R_{2,\mathcal{M}_M,Q_{\mathcal{M}_M}})/L_{\mathcal{M}_M,Q_{\mathcal{M}_M}}$
$p_{Z_{Q_{\mathcal{M}_M}}} = -R_{2,\mathcal{M}_M,Q_{\mathcal{M}_M}}/L_{\mathcal{M}_M,Q_{\mathcal{M}_M}}$
$R_{1,\mathcal{M}_M,Q_{\mathcal{M}_M}} = a_{\mathcal{M}_M,Q_{\mathcal{M}_M}}/(a_{\mathcal{M}_M,Q_{\mathcal{M}_M}} \cdot d_{\mathcal{M}_M,Q_{\mathcal{M}_M}} - b_{\mathcal{M}_M,Q_{\mathcal{M}_M}} \cdot c_{\mathcal{M}_M,Q_{\mathcal{M}_M}})$
$R_{2,\mathcal{M}_M,Q_{\mathcal{M}_M}} = b_{\mathcal{M}_M,Q_{\mathcal{M}_M}} \cdot c_{\mathcal{M}_M,Q_{\mathcal{M}_M}}/(d_{\mathcal{M}_M,Q_{\mathcal{M}_M}} \cdot (b_{\mathcal{M}_M,Q_{\mathcal{M}_M}} \cdot c_{\mathcal{M}_M,Q_{\mathcal{M}_M}} - a_{\mathcal{M}_M,Q_{\mathcal{M}_M}} \cdot d_{\mathcal{M}_M,Q_{\mathcal{M}_M}}))$
$L_{\mathcal{M}_M,Q_{\mathcal{M}_M}} = b_{\mathcal{M}_M,Q_{\mathcal{M}_M}} \cdot c_{\mathcal{M}_M,Q_{\mathcal{M}_M}}/(a_{\mathcal{M}_M,Q_{\mathcal{M}_M}} \cdot d_{\mathcal{M}_M,Q_{\mathcal{M}_M}} - b_{\mathcal{M}_M,Q_{\mathcal{M}_M}} \cdot c_{\mathcal{M}_M,Q_{\mathcal{M}_M}})^2$

It can be proved that $R_{2,\mathcal{M}_M,Q_{\mathcal{M}_M}}$ and $L_{\mathcal{M}_M,Q_{\mathcal{M}_M}}$ are strictly positive, irrespective of $Q_{\mathcal{M}_M}$, whereas R_{1,M,Q_M} admits a negative sign at any operating point $Q_{\mathcal{M}_M}$ corresponding to a NDR bias point $\boldsymbol{P}_{\boldsymbol{\mathcal{M}_M}}$, keeping positive-valued otherwise. Therefore, applying the Local Activity Theorem and the Edge of Chaos Corollary [6], the current-controlled NaMlab memristor is found to work on the Edge of Chaos around some operating point $Q_{\mathcal{M}_M}$ if and only if two inequalities, specifically $p_{Z_{Q_{\mathcal{M}_M}}} < 0$ and $z_{Z_{Q_{\mathcal{M}_M}}} > 0$, hold true simultaneously, which may only apply when $\boldsymbol{P}_{\boldsymbol{\mathcal{M}_M}}$ sits on a NDR branch of the $I_{\mathcal{M}_M,eq}$ versus $V_{\mathcal{M}_M,eq}$ characteristic.

III. THERMALLY-ACTIVATED OSCILLATOR

This section presents the main steps of the systematic methodology adopted for the design of a bio-inspired second-order oscillator, where the only dynamic circuit elements are the two memristors on Edge of Chaos described in sections II.A and II.B, respectively.

A. CIRCUIT TOPOLOGY

In the oscillator of Fig. 3(a), the one-port, featuring terminals A and B, consists of the parallel connection between one NaMLab threshold nano-switch $\mathcal{M}_M$ [5] and the series combination between a PTC thermistor $\mathcal{M}_T$ [12] and a DC voltage source V, and is driven by a bias current source I.

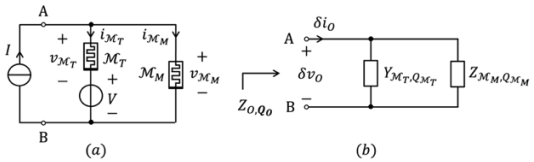

Fig. 3 (a) Thermal oscillator. (b) Local equivalent circuit model of the cell in (a) about an operating point $\boldsymbol{Q_O} = (Q_{\mathcal{M}_T}, Q_{\mathcal{M}_M})$.

A.1 Model

The differential algebraic equation (DAE) set, capturing the bio-inspired operating principles of the proposed second-order reactance-less thermally-activated oscillator, is composed of two ODEs, specifically

$$\dot{T} = \dot{T}(T, v_{\mathcal{M}_M} - V), \text{ and} \quad (9)$$

$$\dot{x} = \dot{x}(x, v_{\mathcal{M}_M}), \quad (10)$$

and one algebraic constraint, namely

$$v_{\mathcal{M}_M} = \frac{I + G_T(T) \cdot V}{G_M(x) + G_T(T)}. \quad (11)$$

A.2 Conditions For the Emergence of Self-Sustained Limit-Cycle Oscillations via Hopf Supercritical Bifurcation

In order for the cell of Fig. 3(a) to undergo infinitesimally-small self-sustained almost-sinusoidal oscillations, originating from a local Hopf Supercritical Bifurcation [13], the bias stimuli V and I should be chosen so as to satisfy the conditions to follow:

1) The DC $I_{\mathcal{M}_M,eq}$ versus $V_{\mathcal{M}_M,eq}$ characteristic of the NaMLab threshold switch crosses the respective nonlinear load line, expressed by

$$I_{\mathcal{M}_M,eq} = I - G_{\mathcal{M}_T}(T_{eq}) \cdot (V_{M,eq} - V), \quad (12)$$

in a *unique point* $\boldsymbol{P}_{\mathcal{M}_M}$, where at least one of the two memristors $\mathcal{M}_T$ and $\mathcal{M}_M$ admits a NDR around the respective operating point.

2) Fixing one of the two bias stimuli, say V, while tuning the other, here I, the poles of the local impedance $Z_{O,\boldsymbol{Q_O}}$ of the oscillator of Fig. 3(a) at the port A - B about its unique operating point, defined as $\boldsymbol{Q_O} \triangleq (Q_{\mathcal{M}_T}, Q_{\mathcal{M}_M})$, form a complex conjugate pair, crossing together the imaginary axis from left to right, as the DC current I attains a specific threshold I_{HB}, signaling the occurrence of a *local Hopf Supercritical Bifurcation* in the proposed bio-inspired circuit.

A case study from one of the three possible scenarios, where, particularly, the crossing point $\boldsymbol{P}_{\mathcal{M}_M}$ between the DC locus of the threshold switch and the associated nonlinear load line triggers NDR effects in both memristors, is described below.

B. CASE STUDY: BOTH DEVICES ON EDGE OF CHAOS

Notions from the principles of Local Activity and Edge of Chaos [6] and techniques from nonlinear circuit and system theory [22] are invoked to determine suitable values for the bias parameters V and I, which, allowing to fulfill both conditions 1) and 2) from section A.2, induce self-sustained oscillations originating out of a local Hopf Supercritical Bifurcation [13] across the proposed bio-inspired all-memristor oscillator of Fig. 3(a) in the scenario where both memristors are poised on NDR bias points. In our exemplary case study, setting V to 0.75V, if and only if I is chosen from the range [52.0716,71.5928]mA, is the thermally-activated oscillator poised on a unique operating point $\boldsymbol{Q_O}$, whose first (second) component Q_T (Q_M) corresponds to a NDR operating point $\boldsymbol{P}_{\mathcal{M}_T}$ ($\boldsymbol{P}_{\mathcal{M}_M}$) for the PTC thermistor (NbO

threshold nano-switch), as indicated in Fig. 4. Applying the Local Activity Theorem [6] to the impedance $Z_{O,\boldsymbol{Q_O}}$ seen at the input port of the circuit of Fig. 3(b) at $\boldsymbol{Q_O}$, as I is decreased from 71.5928mA to 52.0716mA, the cell in Fig. 3(a) is found to transition from the Edge of Chaos operating regime to the instability domain when I descends down to the Hopf Supercritical Bifurcation threshold of $I_{HB} =$ 68.9415mA. Fig. 5 demonstrates the uniqueness of the unstable oscillator operating point, when I is let equal to 55mA, while Fig. 6 visualizes the time evolution of the sustained oscillations, which consequently develop across the cell of Fig. 3(a).

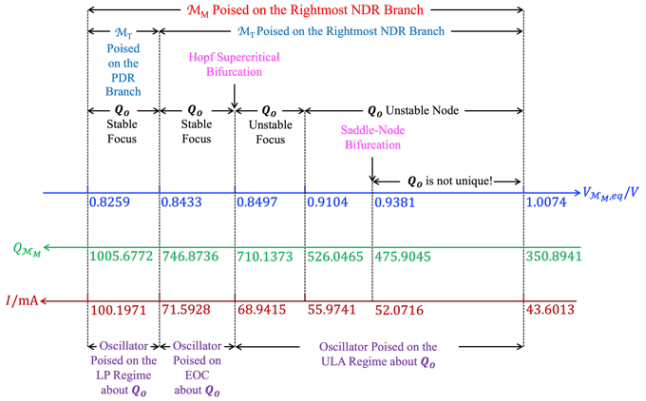

Fig. 4 Unfolding the local behavior of the two-memristor oscillator around an operating point $\boldsymbol{Q_O}$ at which the PTC thermistor (NaMLab memristor) is poised on the rightmost blue (red) branch of its DC current $I_{\mathcal{M}_T,eq}$ ($I_{\mathcal{M}_M,eq}$) versus voltage $V_{\mathcal{M}_T,eq}$ ($V_{\mathcal{M}_M,eq}$) characteristic for $V = 0.75$V. As verified via phase-portrait investigation, as I is decreased from 100.1971mA to 43.6013mA, oscillations are found to emerge across the bio-inspired cell out of a *Hopf Supercritical Bifurcation* when the DC current descends down to 68.9415mA. The cell keeps locked in the oscillatory operating mode for any other smaller DC current until I is decreased down to 52.0716mA, when, with reference to Fig. 5, the minimum of the nonlinear load line becomes tangent to the PDR branch of the NaMLab memristor DC locus, which induces a *Saddle-Node Bifurcation* across the cell of Fig. 3(a), found to admit two additional operating points, one unstable, similarly as $\boldsymbol{Q_O}$, and the other stable, for all lower DC input current I values in the range under sweep.

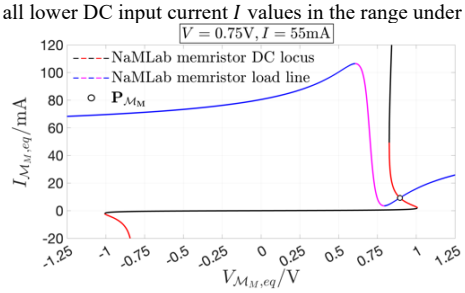

Fig. 5 Determination of the operating point $\boldsymbol{P}_{\mathcal{M}_M} = (V_{M,eq}, I_{M,eq})$ of the threshold switch in the cell from Fig. 3(a) as the crossing (open circle) between the DC I_M versus V_M locus of Fig. 2 and the nonlinear load line from equation (12). Here $V_{M,eq} = 0.917$V and $I_{M,eq} = 7.310$mA. The only oscillator operating point $\boldsymbol{Q_O} = (Q_T, Q_M)$, with $Q_T = 300.000$K and $Q_M = 513.318$, is unstable.

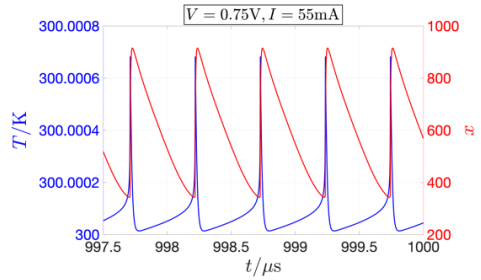

Fig. 6 Blue (red) trace: steady-state oscillatory behaviour of the state of the thermistor (NbOx memristor) in the cell of Fig. 3(a) for $V = 0.75$V and $I =$ 55mA.

IV. CONCLUSIONS

The recent report of a metallic wire, which, when immersed on a physical medium based upon lanthanum cobaltite and biased on the Edge of Chaos, is capable to amplify small-signals without the need to accommodate repeaters along its extension [16] has provided experimental proof of evidence for the extraordinary add-on functionalities, which an otherwise dumb physical system may showcase while poised on a stable yet highly-excitable locally active operating point. This discovery motivates further research on materials blessed with the capability to operate on the Edge of Chaos. Recently we explored the potential of certain volatile memristor physical realizations, featuring a negative differential resistance under suitable polarization, to induce the development of emergent biological phenomena, including spatio-temporal pattern formation ([7], [17]-[18]), across reaction-diffusion cellular neural networks, or to allow the design of innovative bio-plausible electronic neurons ([8], [19]-[20]). In another publication [11] we revealed how an electrical circuit, composed of three resistors, two memristors on Edge of Chaos and two DC voltage sources may undergo symmetry-breaking phenomena, similarly as those observed by Alan Turing in a biological array of reaction cells let interact via diffusion processes, while employing half the number of degrees of freedom relative to the reference system. Yet, the proposed reactance-less circuit was unable to support sustained limit-cycle oscillations on its own. On the other hand, adding just one linear capacitor across a memristor, preliminarily poised on the Edge of Chaos through a simple bias circuit, suffices to trigger the development of oscillations [9] and even chaos [21] across the overall electrical system. In this paper we design a novel all-memristor circuit, which, differently from the electrical network in [11], may lock into an oscillatory operating mode. Powerful concepts from the Local Activity Principle [6] and methods from Bifurcation Theory [22] were employed to derive the conditions necessary for the proposed second-order cell, accommodating just two different physical memristors, featuring in turn a N- and a S-shaped DC characteristic, and a couple of bias sources, of current and voltage form, respectively, to experience a local Hopf supercritical bifurcation [13] spawning infinitesimal quasi-sinusoidal oscillations across its circuitry at steady state. Fundamental to the development of sustained oscillations across the cell is the polarization of at least one of the two memristors along a negative differential resistance branch of the respective DC locus. Importantly, for one of the three admissible scenarios, and precisely when negative differential resistance effects are triggered across both memristors, we demonstrated that the Hopf bifurcation occurs across the proposed all-memristor circuit when the bias parameter setting sets it at the frontier between the highly-excitable Edge of Chaos domain and the instability regime. This work is intended to inspire future studies aiming to the development of robust building blocks [23]-[24], combining Memristors on Edge of Chaos [5] with other groundbreaking nanotechnologies, such as ferroelectric capacitors, admitting a negative differential capacitance under suitable DC stimulation [25], for innovative bio-inspired energy-efficient electronic circuits and systems intended to serve artificial intelligence-based applications.

REFERENCES

[1] A. Ascoli, S. Slesazeck, H. Mähne, R. Tetzlaff, and T. Mikolajick, "Nonlinear dynamics of a locally-active memristor," IEEE Trans. Circuits and Systems—I: Regular Papers, vol. 62, no. 4, pp. 1165-1174, 2015

[2] A.S. Demirkol, A. Ascoli, I. Messaris, and R. Tetzlaff, "Pattern formation dynamics in a Memristor Cellular Nonlinear Network structure with a numerically stable VO_2 memristor model," Japanese Journal of Applied Physics, vol. 61, no. SM0807, pp. 1-11, 2022, DOI: 10.35848/1347-4065/ac8489

[3] I. Messaris, T.D. Brown, A.S. Demirkol, A. Ascoli, M.M. Al Chawa, R.S. Williams, R. Tetzlaff, and L.O. Chua, "NbO2-Mott Memristor: A Circuit-Theoretic Investigation," IEEE Trans. Circuits and Systems-I (TCAS-I): Regular Papers, vol. 68, no. 12, pp. 4979-4992, 2021, DOI: 10.1109/TCSI.2021.3126657

[4] K. Mainzer, and L. Chua, "The Local Activity Principle," Imperial College Press, 2013, 443pp., ISBN-13: 978-1908977090

[5] A. Ascoli, S.A. Demirkol, R. Tetzlaff, S. Slesazeck, T. Mikolajick, and L.O. Chua, "On Local Activity and Edge of Chaos in a NaMLab Memristor," Frontiers in Neuroscience, vol. 15, no. 651452, (30pp.), 2021

[6] L.O. Chua, "Local Activity is the Origin of Complexity," Int. J. on Bifurcation and Chaos, vol. 15, no. 11, pp. 3435–3456, 2005

[7] A. Ascoli, A.S. Demirkol, L. Chua, and R. Tetzlaff, "Edge of Chaos Theory Resolves Smale Paradox," IEEE Trans. Circuits and Systems-I (TCAS-I): Regular Papers, vol. 69, no. 3, pp. 1252-1265, 2022, DOI: 10.1109/TCSI.2021.3133627

[8] A. Ascoli, A.S. Demirkol, I. Messaris, V. Ntinas, D. Prousalis, S. Slesazeck, T. Mikolajick, F. Corinto, M. Bonnin, M. Gilli, P.P. Civalleri, R. Tetzlaff and L. Chua, "Edge of Chaos Theory Unveils the First and Simplest Ever Reported Hodgkin-Huxley Neuristor," Advanced Electronic Materials, 2025, DOI: 10.1002/aelm.202400789

[9] A. Ascoli, A.S. Demirkol, R. Tetzlaff, and L. Chua, "Analysis and Design of Bio-Inspired Circuits with Locally-Active Memristors," IEEE Trans. Circuits and Systems-II (TCAS-II): Express Briefs, vol. 71, no. 3, pp. 1721-1726, March 2024, DOI: 10.1109/TCSII.2023.3339535

[10] https://www.namlab.com

[11] A. Ascoli, A.S. Demirkol, L. Chua, and R. Tetzlaff, "Edge of Chaos is Sine Qua Non for Turing Instability," IEEE Trans. Circuits and Systems-I (TCAS-I): Regular Papers, vol. 69, no. 11, pp. 4596-4609, Nov. 2022, DOI: 10.1109/TCSI.2022.3194465

[12] L. Chua, "If It's Pinched, It's a Memristor", Semiconductor Science and Technology, Special Issue on Memristive Devices, vol. 29, no. 10, (42 pp.), Sept. 2014

[13] A.A. Andronov, and C.E. Chaikin, "Theory of Oscillations," Princeton, NJ, USA: Princeton University Press, 1949

[14] L.O. Chua, "Memristors on Edge of Chaos," Nature Reviews Electrical Engineering, 2024, DOI: 10.1038/s44287-024-00082-1

[15] A.S. Demirkol, A. Ascoli, I. Messaris, and R. Tetzlaff, "Pattern Formation in an RD-MCNN with Locally Active Memristors," in Memristor - An Emerging Device for Post-Moore's Computing and Applications, Yao-Feng Chang ed., IntechOpen Limited, London, 2021, DOI: 10.5772/intechopen.100463

[16] T.D. Brown, A. Zhang, F.U. Nitta, E.D. Grant, J.L. Chong, J. Zhu, S. Radhakrishnan, M. Islam, E.J. Fuller, A.A. Talin, P.J. Shamberger, E. Pop, R.S. Williams, S. Kumar, "Axon-like active signal transmission," Nature, pp. 1-10, 2024, DOI: 10.1038/s41586-024-07921-z

[17] M. Weiher, M. Herzig, R. Tetzlaff, A. Ascoli, T. Mikolajick, and S. Slesazeck, "Pattern formation with local active S-type NbOx memristors," IEEE Trans. Circuits and Systems-I (TCAS-I): Regular Papers, vol. 66, no. 7, pp. 2627-2638, 2019, DOI: 10.1109/TCSI.2019.2894218

[18] A.S. Demirkol, I. Messaris, A. Ascoli, and R. Tetzlaff, "Pattern Formation in an M-CNN Structure Utilizing a Locally Active NbOx memristor", in Memristor Computing Systems, L.O. Chua, R. Tetzlaff, and A. Slavova eds., Springer, 2022, DOI: 10.1007/978-3-030-90582-8

[19] A.S. Demirkol, A. Ascoli, R. Tetzlaff, J.K. Eshraghian, and S.M. Kang, "A Qualitative Approach for the Design of a Locally Active Memristor Based Neuron Circuit," IEEE Int. Conference on Electronics, Circuits and Systems (ICECS), 2023

[20] M.D. Pickett, G. Medeiros-Ribeiro, and R.S. Williams, "A scalable neuristor built with Mott memristors," Nature Materials, vol. 12, no. 2, pp. 114-117, 2013

[21] S. Kumar, J.P. Strachan, and R.S. Williams, "Chaotic dynamics in nanoscale NbO2 Mott memristors for analogue computing," Nature, vol. 548, pp. 318-321, 2017, DOI: 10.1038/nature23307

[22] F. Corinto, M. Forti, and L.O. Chua, "Nonlinear Circuits and Systems with Memristors — Nonlinear Dynamics and Analogue Computing via the Flux-Charge Analysis Method," 438pp., Springer, 2020

[23] S. Kumar, R.S. Williams, and Z. Wang, "Third-order nanocircuit elements for neuromorphic engineering," vol. 585, no. 7826, pp. 518-523, Nature, 2020, DOI: 10.1038/s41586-020-2735-5

[24] A. Ascoli, A.S. Demirkol, I. Messaris, V. Ntinas, D. Prousalis, S. Slesazeck, T. Mikolajick, F. Corinto, M. Bonnin, M. Gilli, P.P. Civalleri, R. Tetzlaff and L. Chua, "A Memristor on Edge of Chaos Enables to Reproduce the Entire Life Cycle of an Action Potential across the Hodgkin-Huxley Neuron in a Three-Element Cell featuring Half the Number of Degrees of Freedom," ACS Nano, 2025, in press

[25] S. Asapu, T. Moon, K. Mahalingam, K.G. Eyink, J.N. Pagaduan, R. Zhao, S. Ganguli, R. Katsumata, Q. Xia, R.S. Williams, and J.J Yang, "Accurate compact nonlinear dynamical model for a volatile ferroelectric ZrO2 capacitor," Nature Partner Journals Unconventional Computing, vol. 1, no. 7, pp. 1-7, 2024, DOI: 10.1038/s44335-024-00007-z